J. Fluid Mech. (1974), *vol.* 65, *part* 3, *pp.* 517–539
Printed in Great Britain

Entry flow in a curved pipe

By M. P. SINGH

Department of Applied Mathematics and Theoretical Physics,
University of Cambridge†

(Received 2 January 1974)

This paper deals with the development of the flow in a curved tube near the inlet. The solution is obtained by the method of matched asymptotic expansions. Two inlet conditions are considered: (i) the condition of constant dynamic pressure at the entrance, which may be of practical interest in applications to blood flow in the aorta; and (ii) a uniform entry condition. It is shown that the geometry and the nature of the entry condition appreciably influence the initial development of the flow. The effect of the secondary flow due to the curvature on the wall shear is discussed and it is shown that the cross-over between shear maxima on the inside and the outside of the tube occurs at a downstream distance which is 1·9 times the radius of the tube for entry condition (i) while in the case of entry condition (ii) it is 0·95 times the radius, which is half the distance required in case (i). It is found that the pressure distribution is not significantly influenced by the secondary flow during the initial development of the motion. The analysis, which is developed for steady motion, can be extended to pulsatile flows, which are of greater physiological interest.

1. Introduction

The character of fluid motion in a bend has been of broad interest both experimentally and theoretically. The first theoretical study of the subject was made by Dean (1927, 1928), who pointed out that the dynamic similarity of the fully developed flow depends on a non-dimensional parameter

$$D = \left(\frac{a}{L}\right)^{\frac{1}{2}} \frac{2aW_m}{\nu}, \tag{1}$$

where W_m is the mean velocity along the pipe, ν the kinematic viscosity and a the radius of the pipe, which is bent in a circle of radius L. Physically, this parameter can be considered as the ratio of the centrifugal force induced by the circular motion of the fluid to the viscous force. The experimental investigations of White (1929) and Adler (1934) show that the ratio γ_c/γ_s of the resistance coefficients (γ_c and γ_s are the resistance coefficients for the curved pipe and for a straight pipe of the same radius respectively) depends only on D as long as the motion is laminar (although this is no longer the case once turbulence has set in). Dean's

† Permanent address: Department of Mathematics, Indian Institute of Technology, New Delhi.

analysis and calculation of the consequent rise in the resistance coefficient were restricted to small values of D. Later, Barua (1963) considered fully developed motion for large D and obtained an approximate solution by a Kármán–Pohlhausen momentum-integral method under the assumption that the motion outside the boundary layer is confined to planes parallel to the plane of symmetry of the pipe. Numerical solutions for laminar flow have been obtained by McConalogue & Srivastava (1968) for moderate values of D and by Greenspan (1973) for the whole range of D.

When a fluid flows through a curved pipe, a pressure gradient directed towards the centre of curvature is set up across the pipe to balance the centrifugal force arising from the curvature. The fluid near the wall of the pipe is moving more slowly than the fluid some way from the wall owing to viscosity and therefore requires a smaller pressure gradient to balance the local centrifugal force. As a result of these different pressure gradients, the faster-flowing fluid moves outwards, whilst the slower-flowing fluid moves inwards. This flow is known as the secondary flow and it is superposed on the main stream. In the case of a circular curved pipe lying in a horizontal plane, the fluid in the middle of the pipe moves outwards and that above and below it moves inwards; thus the resultant flow is helical in the top and bottom halves of the pipe. This pattern of a pair of helices was first theoretically explained by Thompson (1876). The secondary flow has the effect of shifting the high velocity region towards the outer wall and creating a much thicker layer of slowly moving fluid at the inner wall. However, owing to enhanced mixing and momentum transfer due to the secondary flows, the total frictional loss of energy near the wall increases and the fluid experiences more resistance in passing through the pipe.

The process of transition to fully developed curved flow from an initial flow in a straight pipe was studied by Hawthorne (1951). Here we consider a different type of transition, for the case when the curved flow is immediately preceded by an inlet to the curved pipe. Interest in this case has recently developed because of its possible applications to blood flow in the cardiovascular system. In contrast to the requirements of engineering, where the increase in resistance due to curvature is principally sought, a knowledge of the velocity distribution is required in the study of cardiovascular systems so that the distribution of injected substances and effects of the distribution of wall shearing stress on the formation of arterial lesions may be better understood. Very little data exists on the velocity distribution within major arteries, although Seed & Wood (1971) determined the distribution outside the boundary layer within the aorta. Various techniques have been used to measure the instantaneous volume flow rate, but they yield no information on the form of the velocity profile. A theoretical analysis based on fluid-dynamic theory involves many complicated features: viscosity, time dependence of the flow, elastic boundaries, curvature and the complex geometries (see figure 1). Similar difficulties arise in understanding the extent to which turbulent flow exists in arteries. Nerem & Seed (1972) suggested laminar flow in the aorta at Reynolds numbers $Re \lesssim 5000$. Caro, Fitz-Gerald & Schroter (1969) have postulated that low wall shear rates are important in dictating sites of atherogenesis. Similarly, flow regimes are of interest because of the influence on

pressure–flow relations, the generation of audible sounds and mixing and mass-transfer processes. In view of these interests of physiologists, a couple of investigations on entry flow in a curved pipe have been made in recent years. Pickett (1968) adapted the technique used by Atkinson & Goldstein (see Goldstein 1965, p. 304) for flow development in a straight pipe to the case where curvature is present. The inadequacy of this method has been recently pointed out by Van Dyke (1970) and Wilson (1971). Yao (1973) has anaysed the entry flow by taking Barua's model for fully developed flow and assuming that the central cross-flow is parallel to the plane of symmetry. This assumption is questionable, especially near the entry region. Besides, an appropriate choice of the entry conditions is important for the flow in the region close to the entrance. Olson (1971) investigated the entry flow experimentally by considering (i) flat and (ii) parabolic entrance profiles. As was pointed out by Kuchar & Ostrach (1967), it is doubtful whether conditions upstream (in the left ventricle and at the aortic valve) will produce a flat or parabolic velocity profile.

In our analysis, we assume that the dynamic pressure across the cross-section at the entrance to the bend is constant, which is a case of practical interest since it corresponds to the curved pipe taking the fluid from a reservoir at constant pressure. We consider the fluid to be incompressible and viscous. The governing equations of motion in dimensionless form involve three parameters† [see equations (5)–(8)]:

$$\left.\begin{array}{ll} \text{(i) the curvature ratio} & \delta = a/L \sim O(10^{-1}), \\ \text{(ii) the Reynolds number} & Re = a\overline{W}_0/\nu \sim O(10^3), \\ \text{(iii) the frequency parameter} & \epsilon = a\lambda/\overline{W}_0 \sim O(10^{-1}). \end{array}\right\} \tag{2}$$

As the fluid is pumped into the curved pipe from the reservoir (see figure 1), a boundary layer similar to that in a straight pipe develops at the wall. Thus the region consists of two parts: (i) a thin layer near the wall where the viscous forces are balanced by the inertia forces and the centrifugal force has a second-order effect near the inlet and (ii) an inviscid core in which the centrifugal force due to the circular motion of the main body of the fluid along the pipe is balanced by the pressure gradient directed towards the centre of curvature. However, as the flow develops further downstream, the curvature effects become as important as the viscous effects and the inertia forces in the boundary layer, which in turn influence the flow in the core due to displacement. This is in contrast to the flow for small Dean numbers D, in which case the centrifugal force will always be of second order as the fluid flows further downstream. The secondary flow due to curvature consists of the transverse flow of the slower-moving fluid particles in the boundary layer from the outside of the bend towards the inside and the cross-flow of faster-moving fluid particles from inside to the outside of the bend. Thus, the secondary boundary layer behaves as a reservoir receiving the fluid moving

† The estimate of the orders of magnitude of the parameters is obtained from the following data: for the ascending aorta, $a = 1{\cdot}15$–$2{\cdot}18$ cm (for man) or $0{\cdot}50$ cm (for dogs; see McDonald 1960); $\nu = 0{\cdot}038$ cgs units at 37 °C (for man); the duration of each systole (for man) is approximately $0{\cdot}3$ s, during which about 80 ml of blood is pumped from the left ventricle into the ascending aorta. The frequency of the systolic cycle is approximately 70 min^{-1}; λ is 2π times this frequency.

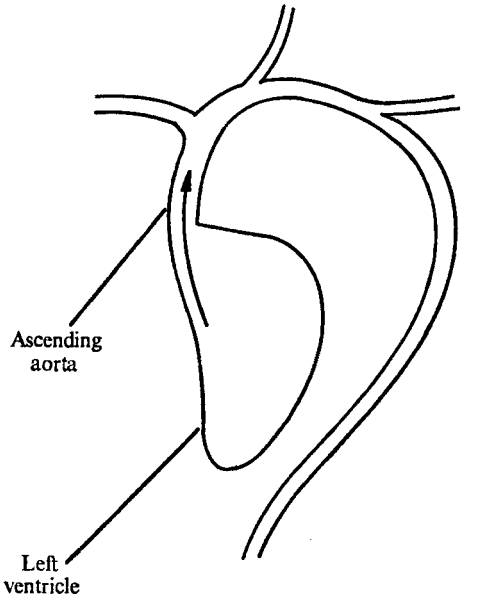

FIGURE 1

towards the outer wall, and also acts as a source because of the fluid leaving it at the inner wall, which is consistent with the mass conservation of the boundary layers in the cross-section of the pipe. The resulting cross-flow forms a stagnation-like flow locally along the outer wall whose convective effect prevents the secondary boundary layer from diffusing further out, and hence it will remain thin as the flow becomes fully developed in contrast to the flow for small Dean number, in which case the boundary layer continues to grow downstream until it fills the tube and the flow becomes fully developed. Further, in view of the enhanced mixing and convective mass transfer due to the secondary flow, the developing flow in a curved tube requires a much shorter entrance length to become fully developed in comparison to a straight tube.

2. Formulation of the problem

Figure 2 shows the system of toroidal co-ordinates (r', α, θ) for the consideration of motion of fluid through a pipe of circular cross-section coiled in the form of a circle. The axis of the circle in which the pipe is coiled is OZ and C is the centre of the cross-section of the pipe in a plane that makes an angle θ with the fixed axial plane. OC is of length L, which is the radius of curvature of the coiled tube. The plane passing through O and perpendicular to OZ will be called the 'central plane' of the pipe and the circle traced out by C its 'central line'. r' denotes the distance CP and α is the angle which CP makes with the line OC produced. Let (u', v', w') denote the corresponding velocity components in the (r', α, θ) directions at time t'.

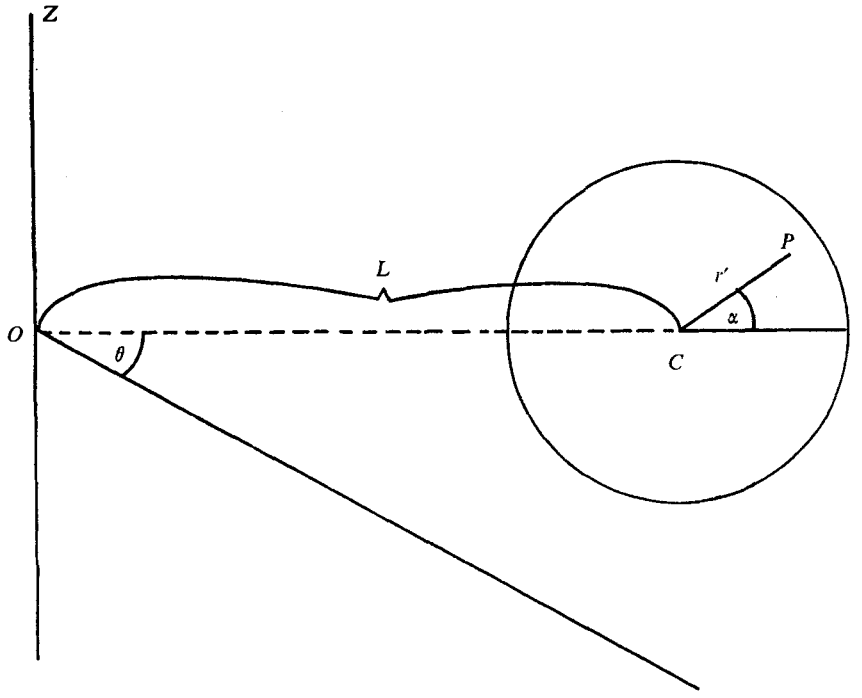

FIGURE 2

Entry and boundary conditions

We shall consider two types of entry conditions.

(*a*) Constant dynamic pressure across the cross-section at the entrance. In this case, the injection velocity is given by

$$\left.\begin{aligned} u' = v' = 0, \\ w' = L\overline{W}_0(1+A\sin\lambda t')/(L+r'\cos\alpha). \end{aligned}\right\} \tag{3}$$

(*b*) Constant injection velocity, i.e., at the entrance to the bend,

$$u' = v' = 0, \quad w' = \overline{W}_0(1+A\sin\lambda t'), \tag{4}$$

and the boundary conditions are

$$u' = v' = w' = 0 \quad \text{at} \quad r' = a. \tag{4a}$$

Non-dimensional equations of motion

Near the entrance, it is natural to refer the velocity to the characteristic entrance velocity $\overline{W}_0$, the co-ordinates r' and s' to a, the pressure to $\rho\overline{W}_0^2$ and time to $1/\lambda$, where $s' = L\theta$ and ρ is the density of the fluid. The governing equations of motion are

$$u_r + \frac{u}{r}\frac{1+2\delta r\cos\alpha}{1+\delta r\cos\alpha} + \frac{v_\alpha}{r} - \frac{\delta v\sin\alpha}{1+\delta r\cos\alpha} + \frac{w_s}{1+\delta r\cos\alpha} = 0, \tag{5}$$

$$\epsilon u_t + uu_r + \frac{vu_\alpha}{r} + \frac{wu_s}{1+\delta r\cos\alpha} - \frac{v^2}{r} - \frac{\delta w^2\cos\alpha}{1+\delta r\cos\alpha}$$
$$= -p_r - \frac{1}{Re}\left[\left(\frac{1}{r}\frac{\partial}{\partial\alpha} - \frac{\delta\sin\alpha}{1+\delta r\cos\alpha}\right)\left(v_r + \frac{v}{r} - \frac{u_\alpha}{r}\right)\right.$$
$$\left. - \frac{u_{ss}}{(1+\delta r\cos\alpha)^2} + \frac{1}{1+\delta r\cos\alpha}\left(w_{rs} + \frac{\delta\cos(\alpha)w_s}{1+\delta r\cos\alpha}\right)\right], \tag{6}$$

$$\epsilon v_t + uv_r + \frac{vv_\alpha}{r} + \frac{wv_s}{1+\delta r\cos\alpha} + \frac{uv}{r} + \frac{\delta w^2\sin\alpha}{1+\delta r\cos\alpha}$$
$$= -\frac{p_\alpha}{r} + \frac{1}{Re}\left[\frac{v_{ss}}{(1+\delta r\cos\alpha)^2} - \frac{w_{s\alpha}}{r(1+\delta r\cos\alpha)} + \frac{\delta w_s\sin\alpha}{(1+\delta r\cos\alpha)^2}\right.$$
$$\left. + \left(\frac{\partial}{\partial r} + \frac{\delta\cos\alpha}{1+\delta r\cos\alpha}\right)\left(v_r + \frac{v}{r} - \frac{u_\alpha}{r}\right)\right], \tag{7}$$

$$\epsilon w_t + uw_r + \frac{\delta uw\cos\alpha}{1+\delta r\cos\alpha} + \frac{vw_\alpha}{r} - \frac{\delta vw\sin\alpha}{1+\delta r\cos\alpha} + \frac{ww_s}{1+\delta r\cos\alpha}$$
$$= -\frac{p_s}{1+\delta r\cos\alpha} + \frac{1}{Re}\left[\left(\frac{\partial}{\partial r} + \frac{1}{r}\right)\left(w_r + \frac{\delta w\cos\alpha}{1+\delta r\cos\alpha}\right) + \frac{W_{\alpha\alpha}}{r^2} - \frac{1}{r}\frac{\partial}{\partial\alpha}\left(\frac{\delta w\sin\alpha}{1+\delta r\cos\alpha}\right)\right.$$
$$\left. - \left(\frac{\partial}{\partial r} + \frac{1}{r}\right)\frac{u_s}{1+\delta r\cos\alpha} - \frac{1}{r}\frac{\partial}{\partial\alpha}\left(\frac{v_s}{1+\delta r\cos\alpha}\right)\right], \tag{8}$$

where the unprimed variables are in dimensionless form and the parameters ϵ, δ and Re are defined in (2).

It may be noted that, in the absence of viscosity, the exact solution of the above equations satisfying the entry condition (3) is

$$\left.\begin{aligned} &u = v = 0, \quad w = (1 + A\sin t)/(1+\delta r\cos\alpha), \\ &p = -\frac{1}{2}\frac{(1+A\sin t)^2}{(1+\delta r\cos\alpha)^2} - \epsilon As\cos t. \end{aligned}\right\} \tag{9}$$

Steady entry problem

We shall now limit our discussion to the steady case. Since $\epsilon \sim O(10^{-1})$, this analysis can later be extended to the quasi-steady situation in a straightforward manner.

The governing equations are (5)–(8) with terms containing time derivatives dropped and the following conditions are to be satisfied. First,

$$u = v = 0, \quad w = 1/(1+\delta r\cos\alpha) \quad \text{at} \quad s = 0, \tag{10}$$

which corresponds to the condition of constant dynamic pressure at the entrance to the bend. The solution for the uniform entry condition problem can be obtained from this discussion after some minor modifications and will be given at the end of this analysis. Second,

$$u = v = w = 0 \quad \text{at} \quad r = 1. \tag{11}$$

3. Solution

As the fluid is injected into the pipe, the central core of the fluid will not be influenced by viscosity, whose effects will be confined to a thin layer near the wall of the pipe. The flow can, therefore, be considered to be divided into two regions: (i) an inviscid core in which the centrifugal force due to the curved motion of the main body of the fluid along the pipe is balanced by the pressure gradient directed towards the centre of curvature and (ii) a thin boundary layer in which the viscous forces are balanced by inertia forces. As in the classical boundary layer, pressure will be impressed on the flow in the boundary layer by the external flow, which implies that the azimuthal pressure gradient, which is of second order in the initial stages of motion, will induce a transverse flow in the boundary layer from the outside of the bend towards the inside. The effect of the growing boundary layer on the flow in the core will be to accelerate the motion due to the displacement effect of the boundary layer, and the effect of the second-order transverse flow in the boundary layer will be to induce a cross-flow from the inside of the bend towards outside to satisfy the mass conservation principle. The analysis shows that the secondary flow due to the curvature effects in the region close to the entry can be obtained by perturbing the solution for developing flow in a straight tube.

First-order solution in the inviscid core

The solution in the core is just the undisturbed entry flow

$$\left.\begin{aligned} u = v = 0, \quad w = 1/(1+\delta r\cos\alpha), \\ p = -1/2(1+\delta r\cos\alpha)^2. \end{aligned}\right\} \tag{12}$$

First-order boundary layer

In view of the above analysis, we magnify the radial co-ordinate r, which is very small in the thin boundary layer. Accordingly, we introduce, as in the classical boundary layer,

$$\left.\begin{aligned} r = 1-\beta\eta, \quad u = \beta\tilde{u}, \quad \text{where} \quad \beta = Re^{-\frac{1}{2}}, \\ v(r,\alpha,s,\beta,\delta) = \tilde{v}(\eta,\alpha,s,\beta,\delta), \text{ etc.} \end{aligned}\right\} \tag{13}$$

Further we assume that

$$\left.\begin{aligned} \tilde{u}(\eta,\alpha,s,\beta,\delta) = \tilde{u}_0(\eta,\alpha,s,\delta)+O(\beta^a),\dagger \quad a>0, \\ \tilde{u}_0(\eta,\alpha,s,\delta) = \tilde{u}_{00}(\eta,\alpha,s)+\delta\tilde{u}_{01}(\eta,\alpha,s)+O(\delta^2) \end{aligned}\right\} \tag{14}$$

and similar expansions would hold for $\tilde{v}$, $\tilde{w}$ and $\tilde{p}$. Here $\tilde{u}_{00}$ is the corresponding straight-tube solution and $\tilde{u}_{01}$ is the curvature effect.

† The order of the term after $\tilde{u}_0$ would be determined by applying the condition for matching with the flow in the inviscid core due to displacement. The subsequent analysis would show that $a = 1$.

$O(1)$ equations, matching and boundary conditions

In view of (13) and (14), we obtain the following equations from (5)–(8):

$$-\tilde{u}_{00\eta}+\tilde{v}_{00\alpha}+\tilde{w}_{00s}=0, \tag{15}$$

$$\tilde{p}_{00\eta}=0, \tag{16}$$

$$-\tilde{u}_{00}\tilde{v}_{00\eta}+\tilde{v}_{00}\tilde{v}_{00\alpha}+\tilde{w}_{00}\tilde{v}_{00s}=-\tilde{p}_{00\alpha}+\tilde{v}_{00\eta\eta}, \tag{17}$$

$$-\tilde{u}_{00}\tilde{w}_{00\eta}+\tilde{v}_{00}\tilde{w}_{00\alpha}+\tilde{w}_{00}\tilde{w}_{00s}=-\tilde{p}_{00s}+\tilde{w}_{00\eta\eta}. \tag{18}$$

The appropriate boundary conditions are

$$\tilde{u}_{00}=\tilde{v}_{00}=\tilde{w}_{00}=0 \quad \text{at} \quad \eta=0 \tag{19}$$

and the condition for matching with the undisturbed inviscid flow yields

$$\tilde{v}_{00}\to 0, \quad \tilde{w}_{00}\to 1 \quad \text{as} \quad \eta\to\infty, \tag{20}$$

which also holds at $s=0$.

From (16), we find that the pressure is impressed on the boundary layer by the external flow and so the pressure-gradient terms drop out of (17) and (18). The matching condition (20) suggests that $\tilde{w}_{00}$ is a function only of η and s. This implies that $\tilde{v}_{00}$ satisfies a homogeneous equation and homogeneous boundary condition and so the solution is

$$\tilde{v}_{00}\equiv 0. \tag{21}$$

$\tilde{u}_{00}$ and $\tilde{w}_{00}$ now satisfy the usual Blasius-type equations and boundary conditions and so we introduce

$$\zeta=\eta/(2s)^{\frac{1}{2}}, \quad \tilde{\psi}_{00}=(2s)^{\frac{1}{2}}f_{00}(\zeta), \tag{22}$$

where $\tilde{\psi}_{00}$ is the stream function:

$$\tilde{u}_{00}=\tilde{\psi}_{00s}, \quad \tilde{w}_{00}=\tilde{\psi}_{00\eta}. \tag{23}$$

Thus, we have

$$f_{00}'''+f_{00}f_{00}''=0, \tag{24a}$$

with boundary conditions

$$f_{00}(0)=f_{00}'(0)=0, \quad f_{00}'(\infty)=1, \tag{24b}$$

which is the familiar problem solved by Blasius for the flow along a flat plate.

$O(\delta)$ equations, matching and boundary conditions

The governing equations, are from (5)–(8),

$$-\tilde{u}_{01\eta}+\tilde{v}_{01\alpha}+\tilde{w}_{01s}-\tilde{w}_{00s}\cos\alpha=0. \tag{25}$$

$$\tilde{p}_{01\eta}=0, \tag{26}$$

$$-\tilde{u}_{00}\tilde{v}_{01\eta}+\tilde{w}_{00}\tilde{v}_{01s}+\tilde{w}_{00}^2\sin\alpha=-\tilde{p}_{01\alpha}+\tilde{v}_{01\eta\eta}, \tag{27}$$

$$-\tilde{u}_{00}\tilde{w}_{01\eta}-\tilde{u}_{01}\tilde{w}_{00\eta}+\tilde{w}_{00}\tilde{w}_{01s}+\tilde{w}_{01}\tilde{w}_{00s}-\tilde{w}_{00}\tilde{w}_{00s}\cos\alpha=-\tilde{p}_{01s}+\tilde{w}_{01\eta\eta}. \tag{28}$$

The boundary conditions are

$$\tilde{u}_{01}=\tilde{v}_{01}=\tilde{w}_{01}=0 \quad \text{at} \quad \eta=0 \tag{29}$$

and the condition for matching with the inviscid flow in the core is

$$\tilde{v}_{01}\to 0, \quad \tilde{w}_{01}\to -\cos\alpha \quad \text{as} \quad \eta\to\infty, \tag{30}$$

which also holds at $s=0$.

Again the pressure is impressed on the boundary layer by the external flow, and from (12) we find that

$$\tilde{p}_{01} = \cos\alpha. \tag{31}$$

Hence, the pressure gradient and the centrifugal force have only a second-order effect in the boundary layer during the initial stages of the motion.

Equation (27) and the pressure given by (31) suggest that

$$\tilde{v}_{01}(\eta, \alpha, s) = \tilde{V}_{01}(\eta, s)\sin\alpha, \tag{32}$$

and hence, from (25), it follows that

$$\tilde{u}_{01}(\eta, \alpha, s) = \tilde{U}_{01}(\eta, s)\cos\alpha, \quad \tilde{w}_{01}(\eta, \alpha, s) = \tilde{W}_{01}(\eta, s)\cos\alpha. \tag{33}$$

Equations (25)–(28) now reduce to

$$-\tilde{U}_{01\eta} + \tilde{V}_{01} + \tilde{W}_{01s} - \tilde{w}_{00s} = 0, \tag{34}$$

$$\tilde{V}_{01\eta\eta} + \tilde{u}_{00}\tilde{V}_{01\eta} - \tilde{w}_{00}\tilde{V}_{01s} = \tilde{w}_{00}^2 - 1, \tag{35}$$

$$\tilde{W}_{01\eta\eta} + \tilde{u}_{00}\tilde{W}_{01\eta} - \tilde{w}_{00}\tilde{W}_{01s} + \tilde{U}_{01}\tilde{w}_{00\eta} - \tilde{W}_{01}\tilde{w}_{00s} + \tilde{w}_{00}\tilde{w}_{00s} = 0 \tag{36}$$

and the corresponding boundary and matching conditions become

$$\tilde{U}_{01} = \tilde{V}_{01} = \tilde{W}_{01} = 0 \quad \text{at} \quad \eta = 0, \tag{37}$$

$$\tilde{V}_{01} \to 0, \quad \tilde{W}_{01} \to -1 \quad \text{as} \quad \eta \to \infty. \tag{38}$$

(The latter two conditions also hold at $s = 0$.) Again, we introduce stream functions $\tilde{\psi}_{01}$ and $\tilde{\phi}_{01}$ such that

$$\tilde{V}_{01} = \tilde{\phi}_{01\eta}, \quad \tilde{W}_{01} = \tilde{\psi}_{01\eta} + \tilde{\psi}_{00\eta}, \quad \tilde{U}_{01} = \tilde{\psi}_{01s} + \tilde{\phi}_{01}. \tag{39}$$

The governing equations and conditions (38) suggest that

$$\left.\begin{aligned} \tilde{\phi}_{01}(\eta, s) &= (2s)^{\frac{1}{2}} s g_{01}(\zeta), \\ \tilde{\psi}_{01}(\eta, s) &= (2s)^{\frac{1}{2}}[f_{01}(\zeta) + s^2 f_{02}(\zeta)]. \end{aligned}\right\} \tag{40}$$

The appropriate equations are now

$$\left.\begin{aligned} &f_{01}''' + f_{00}f_{01}'' + f_{00}''f_{01} = 0, \\ \text{with} \quad &f_{01}(0) = f_{01}'(0) = 0, \quad f_{01}'(0) \to -2 \quad \text{as} \quad \zeta \to \infty; \end{aligned}\right\} \tag{41}$$

$$\left.\begin{aligned} &f_{02}''' + f_{00}f_{02}'' - 4f_{00}'f_{02}' + f_{00}''(2g_{01} + 5f_{02}) = 0, \\ \text{with} \quad &f_{02}(0) = f_{02}'(0) = 0, \quad f_{02}'(\zeta) \to 0 \quad \text{as} \quad \zeta \to \infty; \end{aligned}\right\} \tag{42}$$

$$\left.\begin{aligned} &g_{01}''' + f_{00}g_{01}'' - 2f_{00}'g_{01}' = 2(f_{00}'^2 - 1), \\ \text{with} \quad &g_{01}(0) = g_{01}'(0) = 0, \quad g_{01}'(\zeta) \to 0 \quad \text{as} \quad \zeta \to \infty. \end{aligned}\right\} \tag{43}$$

This is a system of linear ordinary differential equations whose numerical solution can be determined in a straightforward manner. In fact, the solution of (41) can be expressed in terms of f_{00} and is given by

$$f_{01} = -[f_{00} + \zeta f_{00}']. \tag{44}$$

The first-order boundary-layer solution is therefore given by

$$\tilde{w}_0 = f'_{00} + \delta\cos\alpha[f'_{00} + f'_{01} + s^2 f'_{02}] + O(\delta^2), \tag{45}$$

$$\tilde{v}_0 = \delta\sin(\alpha)\, s g'_{01} + O(\delta^2), \tag{46}$$

$$\tilde{u}_0 = (2s)^{-\frac{1}{2}}[f_{00} - \zeta f'_{00} + \delta\cos\alpha(2s^2 g_{01} + 5s^2 f_{02} - \zeta s^2 f'_{02} + f_{01} - \zeta f'_{01})] + O(\delta^2), \tag{47}$$

which shows that the curvature effect, which is of second order initially, becomes larger as the flow proceeds further downstream. When $s = O(\delta^{-\frac{1}{2}})$, the curvature effect becomes as important as the viscous and inertia forces in the boundary layer. In fact the above analysis is no longer valid when $s = O(\delta^{-\frac{1}{2}})$. In a subsequent paper, we shall discuss the flow development in this region and further downstream and show how the fully developed flow is approached. We shall, therefore, confine our analysis in this discussion to the flow in the region close to the entry.

Flow due to displacement

We find that the radial component $\tilde{u}$ has not been matched with the corresponding undisturbed inviscid core velocity, which induces a second-order flow in the core. Now, as $\zeta \to \infty$,

$$\tilde{u} \equiv u/\beta \sim (2s)^{-\frac{1}{2}}\{-\beta_1 + \delta\cos\alpha[\beta_3 + s^2(2\beta_2 + 5\beta_4)]\}, \tag{48}$$

where

$$\left.\begin{aligned} \beta_1 &= \lim_{\zeta\to\infty}(\zeta - f_{00}) = 1{\cdot}21678, \\ \beta_2 &= \lim_{\zeta\to\infty} g_{01} = 1{\cdot}139274, \\ \beta_3 &= \lim_{\zeta\to\infty}(f_{01} + 2\zeta) = 1{\cdot}21678, \\ \beta_4 &= \lim_{\zeta\to\infty} f_{02} = 0{\cdot}522839. \end{aligned}\right\} \tag{49}$$

This suggests that the flow field in the core will be of the form

$$\left.\begin{aligned} u(r,\alpha,s,\beta,\delta) &= \beta u_1(r,\alpha,s,\delta) + O(\beta^{1+b}),\dagger \quad b > 0, \\ v(r,\alpha,s,\beta,\delta) &= \beta v_1(r,\alpha,s,\delta) + O(\beta^{1+b}), \\ w(r,\alpha,s,\beta,\delta) &= 1/(1+\delta r\cos\alpha) + \beta w_1(r,\alpha,s,\delta) + O(\beta^{1+b}), \\ p(r,\alpha,s,\beta,\delta) &= -1/(2(1+\delta r\cos\alpha)^2 + \beta p_1(r,\alpha,s,\delta) + O(\beta^{1+b}). \end{aligned}\right\} \tag{50}$$

We further assume that

$$u_1(r,\alpha,s,\delta) = u_{10}(r,\alpha,s) + \delta u_{11}(r,\alpha,s) + O(\delta^2) \tag{51}$$

and similar expansions for v_1, w_1 and p_1. Here, u_{10} is the straight-tube effect and u_{11} represents the curvature effect.

From (5)–(8), we obtain the following equations.

At $O(\beta)$

$$u_{10r} + u_{10}/r + v_{10\alpha}/r + w_{10s} = 0, \tag{52}$$

$$u_{10s} = -p_{10r}, \quad v_{10s} = -r^{-1}p_{10\alpha}, \quad w_{10s} = -p_{10s}. \tag{53)–(55}$$

† The order of the next term after βu_1 would be determined by applying the condition for matching with the solution of appropriate order in the second-order boundary layer.

The appropriate matching condition from (48) is given by

$$u_{10} = -\beta_1/(2s)^{\frac{1}{2}} \quad \text{at} \quad r = 1, \tag{56a}$$

and the entry conditions are

$$p_{10} = w_{10} = 0 \quad \text{at} \quad s = 0. \tag{56b}$$

At $O(\beta\delta)$

$$u_{11r} + u_{11}/r + u_{10}\cos\alpha + v_{11\alpha}/r - v_{10}\sin\alpha + w_{11s} - r\cos(\alpha)\, w_{10s} = 0, \tag{57}$$

$$u_{11s} - 2r\cos(\alpha)\, u_{10s} - 2\cos(\alpha)\, w_{10} = -p_{11r}, \tag{58}$$

$$v_{11s} - 2r\cos(\alpha)\, v_{10s} + 2\sin(\alpha)\, w_{10} = -r^{-1}p_{11\alpha}, \tag{59}$$

$$w_{11s} - 2r\cos(\alpha)\, w_{10s} = -p_{11s} + r\cos(\alpha)\, p_{10s}. \tag{60}$$

The matching condition (48) yields

$$u_{11} = \cos\alpha(2s)^{-\frac{1}{2}}[\beta_3 + s^2(2\beta_2 + 5\beta_4)] \quad \text{at} \quad r = 1 \tag{61a}$$

and the entry conditions are

$$p_{11} = w_{11} = 0 \quad \text{at} \quad s = 0. \tag{61b}$$

Solution of $O(\beta)$ equations

Integrating (55) with respect to s and using (56b), we obtain

$$p_{10} = -w_{10}. \tag{62}$$

Condition (56a) suggests that

$$p_{10}(r, \alpha, s) \equiv p_{10}(r, s), \tag{63}$$

which implies that

$$v_{10} \equiv 0 \tag{64}$$

and

$$p_{10rr} + r^{-1}p_{10r} + p_{10ss} = 0. \tag{65}$$

Fourier sine transformation yields the solution which satisfies (56):

$$p_{10} = -\frac{\beta_1}{\pi^{\frac{1}{2}}}\int_0^\infty \frac{\sigma^{-\frac{1}{2}} I_0(\sigma r)}{I_1(\sigma)} \sin\sigma s\, d\sigma, \tag{66}$$

which represents the effect of displacement due to the boundary layer in the case of a straight tube.

Solution of $O(\beta\delta)$ equations

The matching condition (61a) and (57)–(60) suggest that

$$\left.\begin{aligned} u_{11}(r, \alpha, s) &= U_{11}(r, s)\cos\alpha, \quad v_{11}(r, \alpha, s) = V_{11}(r, s)\sin\alpha, \\ w_{11}(r, \alpha, s) &= W_{11}(r, s)\cos\alpha, \quad p_{11}(r, \alpha, s) = P_{11}(r, s)\cos\alpha. \end{aligned}\right\} \tag{67}$$

Integrating (60) with respect to s, using (62), (66) and the entry condition (61b), we obtain

$$W_{11} - rw_{10} = -P_{11}. \tag{68}$$

Equations (58) and (59) now yield

$$U_{11s} = -P_{11r} + 2w_{10} + 2ru_{10s}, \tag{69}$$

$$rV_{11s} = P_{11} - 2rw_{10}, \tag{70}$$

and hence, from (57), we obtain

$$P_{11rr}+P_{11r}/r-P_{11}/r^2+P_{11ss}=7w_{10r}+2rw_{10rr}. \tag{71}$$

Again, using Fourier sine transformation, the solution of (71) satisfying (61) is

$$\begin{aligned}P_{11}=\frac{1}{2\pi^{\frac{1}{2}}}\int_0^\infty \frac{\sin\sigma s\,d\sigma}{I_1(\sigma)}\Big[&\frac{I_1(\sigma r)}{I_0(\sigma)+I_2(\sigma)}(-3\sigma^{-\frac{1}{2}}(2\beta_2+5\beta_4)I_1(\sigma)\\&-2\sigma^{-\frac{3}{2}}\beta_1 I_0(\sigma)-4\sigma^{-\frac{1}{2}}\beta_1 I_1(\sigma)+4\sigma^{-\frac{1}{2}}\beta_3 I_1(\sigma)-2\beta_1\sigma^{\frac{1}{2}}I_0(\sigma))\\&+\beta_1(\sigma^{\frac{1}{2}}r^2I_1(\sigma r)+5\sigma^{-\frac{1}{2}}rI_0(\sigma r))\Big].\end{aligned} \tag{72}$$

The analysis can be extended systematically to obtain higher-order terms of the solution in the boundary layer and the core.

4. Results and discussion

Boundary layer

$$\tilde{w}_0=f'_{00}+\delta\cos\alpha(f'_{00}+f'_{01}+s^2f'_{02})+O(\delta^2). \tag{73}$$

Here, the first term on the right-hand side is the Blasius boundary-layer term and the second term represents the curvature effect; the first two terms inside the brackets represent the variation of the Blasius boundary layer with α due to (i) dependence on α of the flow velocity just outside the boundary layer and (ii) dependence on α of the distance traversed along the curved wall for given s respectively, and the last term represents the development of the secondary flow. The solution shows how the curvature effect, which is initially of second order, grows as the fluid flows further downstream. A similar interpretation can be given for the other components:

$$\tilde{v}_0=\delta\sin(\alpha)\,sg'_{01}+O(\delta^2), \tag{74}$$

$$\tilde{u}_0=(2s)^{-\frac{1}{2}}\{f_{00}-\zeta f'_{00}+\delta\cos\alpha[f_{01}-\zeta f'_{01}+s^2(2g_{01}+5f_{02}-\zeta f'_{02})]\}+O(\delta^2). \tag{75}$$

The axial skin friction is given by

$$\begin{aligned}\tau_{ws}&=-(\mu\rho\bar{W}_0^3/2as)^{\frac{1}{2}}[f''_{00}(0)+\delta\cos\alpha(f''_{00}(0)+f''_{01}(0)+s^2f''_{02}(0))]\\&=-(\mu\rho\bar{W}_0^3/2as)^{\frac{1}{2}}[0{\cdot}4696+\delta\cos\alpha(0{\cdot}2562s^2-0{\cdot}9392)].\end{aligned} \tag{76}$$

Here, the first term is the skin friction for the straight tube and the next terms represent the curvature effect, which is of second order initially but grows as the flow develops further downstream. The second term is the effect of the secondary velocity and the last term is the effect of reduced/increased external flow and the longer/shorter wall length traversed by the fluid at the outside/inside of the bend. Since the effect of the secondary velocity on the skin friction is initially small, the fluid experiences less resistance in the outer part of the bend in comparison with the straight-tube value owing to the reduced external flow and the longer wall length and it experiences increased resistance initially at the inside of the bend owing to the increased external flow and shorter wall length. The boundary layer of retarded fluid is growing all round the tube but the effect of the secondary flow, which increases with downstream distance, is that at the outside of the

bend it thins the boundary layer because retarded fluid is drawn off in the azimuthal direction, which results in reduced displacement and increased skin friction. On the other hand, the situation will be reversed for the inner side of the bend because the secondary flow brings in additional retarded fluid and thickens the boundary layer, which results in increased displacement and consequently a decrease in skin friction. Thus the cross-over (the point where the effect of secondary velocity just overcomes the effect of reduced/increased external flow and longer/shorter wall length on the skin friction at the outside/inside of the bend) occurs at

$$s \simeq 1{\cdot}9, \tag{77}$$

a position 1·9 radii from the inlet, which is independent of the curvature of the tube as well as the Reynolds number of the flow. The azimuthal skin friction is given by

$$\tau_{w\alpha} = -(\rho\mu\overline{W}_0^3/2as)^{\frac{1}{2}}\,\delta\sin(\alpha)\,sg''_{01}(0), \tag{78}$$

where $g''_{01}(0) = 1{\cdot}535795$, which increases as the fluid flows further downstream. The mean drag coefficient C_D, defined by

$$C_D = -\int_0^l\int_{\alpha_1}^{\alpha_2}\tau_{ws}a\,d\alpha\,ds \Big/ \tfrac{1}{2}\rho\overline{W}_0^2\,\pi a l$$

(where for the outside of the bend $\alpha_1 = -\frac{1}{2}\pi$ and $\alpha_2 = \frac{1}{2}\pi$, and for the inside $\alpha_1 = \frac{1}{2}\pi$ and $\alpha_2 = \frac{3}{2}\pi$), is given by

$$C_D = 2(2/Re)^{\frac{1}{2}}[f''_{00}(0) \pm (2\delta/\pi)(f''_{00}(0) + f''_{01}(0) + \tfrac{1}{5}l^2 f''_{02}(0)]\,l^{-\frac{1}{2}} \tag{79}$$

for the outside or inside wall, where l is the length of the tube and

$$f''_{00}(0) = 0{\cdot}4696, \quad f''_{01}(0) = -1{\cdot}4088, \quad f''_{02}(0) = 0{\cdot}2562.$$

The equation for the limiting streamlines at the wall can be written as

$$\frac{d\alpha}{ds} = \lim_{r\to 1}\frac{v}{w} = \lim_{r\to 1}\frac{v_r}{w_r} = \frac{\tau_{w\alpha}}{\tau_{ws}},$$

therefore

$$\frac{d\alpha}{ds} = \frac{\delta\sin(\alpha)\,sg''_{01}(0)}{f''_{00}(0) + \delta\cos\alpha[f''_{00}(0) + f''_{01}(0) + s^2 f''_{02}(0)]}. \tag{80}$$

These streamlines are plotted in figure 3.

Inviscid core

$$\begin{aligned} p = [-\tfrac{1}{2} + \delta r\cos\alpha + O(\delta^2)] + \frac{\beta}{2\pi^{\frac{1}{2}}}\int_0^\infty \frac{\sin\sigma s\,d\sigma}{I_1(\sigma)}\Big[& -2\beta_1\sigma^{-\frac{1}{2}}I_0(\sigma r) \\ & + \delta\cos\alpha\Big\{\frac{I_1(\sigma r)}{I_0(\sigma)+I_2(\sigma)}(-3\sigma^{-\frac{5}{2}}(2\beta_2+5\beta_4)I_1(\sigma) - 2\sigma^{-\frac{3}{2}}\beta_1 I_0(\sigma) \\ & - 4\sigma^{-\frac{1}{2}}\beta_1 I_1(\sigma) + 4\sigma^{-\frac{1}{2}}\beta_3 I_1(\sigma) - 2\beta_1\sigma^{\frac{1}{2}}I_0(\sigma)) \\ & + \beta_1(\sigma^{\frac{1}{2}}r^2 I_1(\sigma r) + 5\sigma^{-\frac{1}{2}}rI_0(\sigma r))\Big\} + O(\delta^2)\Big]. \end{aligned} \tag{81}$$

Here, the first term $-\frac{1}{2} + \delta r\cos\alpha + O(\delta^2)$ is the pressure needed to maintain the flow pattern under the centrifugal force and the second term, the integral, represents the displacement effects of the boundary layer and the influence of the secondary flow. The first term in the integral is the solution for a straight tube and

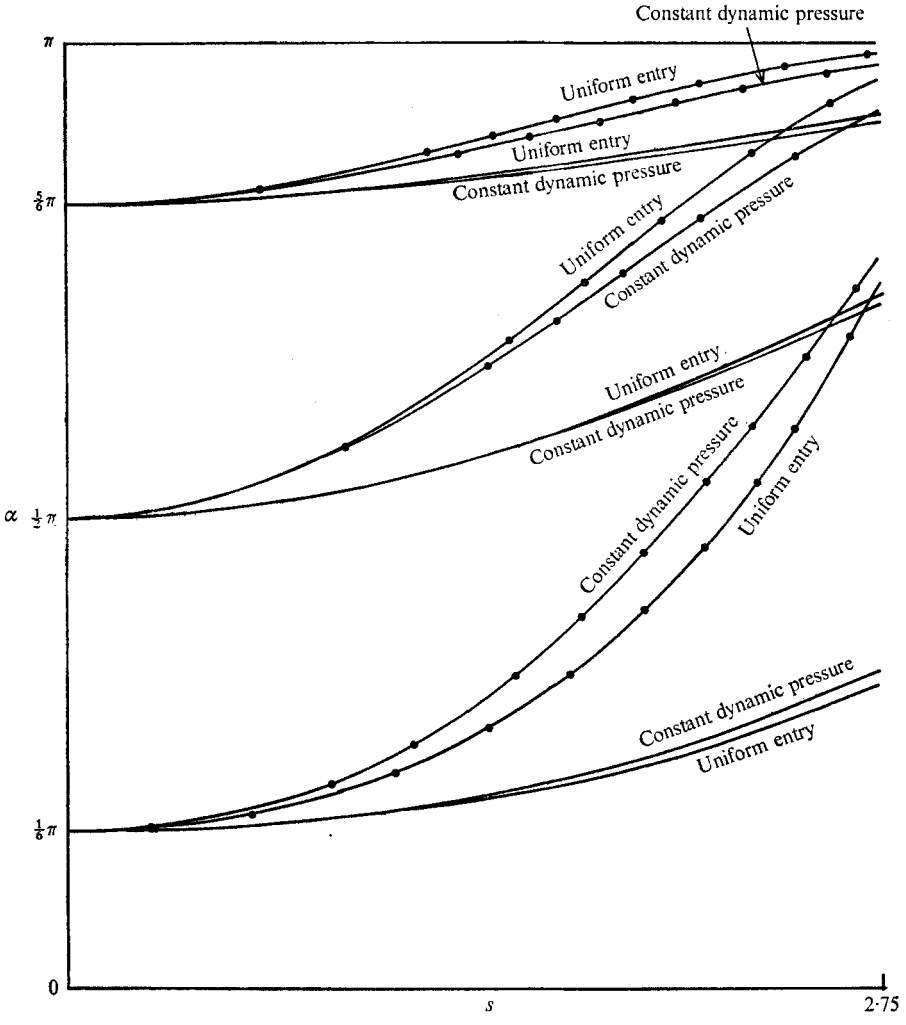

FIGURE 3. Limiting streamlines. ——, $\delta = \frac{1}{16}$; —●—, $\delta = \frac{1}{6}$.

represents the pressure required to accelerate the flow along the tube owing to the displacement effect of the boundary layer; the second term in the integral represents the interaction between the cross-flow and the accelerating flow.

A similar interpretation can be given to the expression for the velocity components:

$$w = 1 - \delta r\cos\alpha + O(\delta^2) + \frac{\beta}{2\pi^{\frac{1}{2}}}\int_0^\infty \frac{\sin\sigma s\, d\sigma}{I_1(\sigma)}\Big[2\beta_1\sigma^{-\frac{1}{2}}I_0(\sigma r) + \delta\cos\alpha\Big\{\frac{I_1(\sigma r)}{I_0(\sigma)+I_2(\sigma)}\,(3\sigma^{-\frac{3}{2}}(2\beta_2+5\beta_4)I_1(\sigma) + 2\sigma^{-\frac{3}{2}}\beta_1 I_0(\sigma) + 4\sigma^{-\frac{1}{2}}\beta_1 I_1(\sigma) - 4\sigma^{-\frac{1}{2}}\beta_3 I_1(\sigma) + 2\beta_1\sigma^{\frac{1}{2}}I_0(\sigma)) - \beta_1(\sigma^{\frac{1}{2}}r^2 I_1(\sigma r) + 3\sigma^{-\frac{1}{2}}rI_0(\sigma r))\Big\} + O(\delta^2)\Big], \qquad (82)$$

$$v = \frac{\beta\delta\sin\alpha}{2\pi^{\frac{1}{2}}r}\int_0^\infty \frac{-\cos\sigma s\,d\sigma}{\sigma I_1(\sigma)}\left[\frac{I_1(\sigma r)}{I_0(\sigma)+I_2(\sigma)}\{-3\sigma^{-\frac{5}{2}}(2\beta_2+5\beta_4)I_1(\sigma) - 2\sigma^{-\frac{3}{2}}\beta_1 I_0(\sigma) - 4\sigma^{-\frac{1}{2}}\beta_1 I_1(\sigma) + 4\sigma^{-\frac{1}{2}}\beta_3 I_1(\sigma) - 2\beta_1\sigma^{\frac{1}{2}}I_0(\sigma)\} + \beta_1\{\sigma^{\frac{1}{2}}r^2 I_1(\sigma r) + \sigma^{-\frac{1}{2}}r I_0(\sigma r)\}\right] + O(\beta\delta^2), \tag{83}$$

$$u = \frac{\beta}{4\pi^{\frac{1}{2}}}\int_0^\infty \frac{-\cos\sigma s\,d\sigma}{\sigma I_1(\sigma)}\left[4\beta_1\sigma^{\frac{1}{2}}I_1(\sigma r) + \delta\cos\alpha\left\{-2\beta_1(2\sigma^{\frac{1}{2}}rI_1(\sigma r) + \sigma^{-\frac{1}{2}}I_0(\sigma r) + \sigma^{\frac{3}{2}}r^2 I_0(\sigma r)) + \frac{I_0(\sigma r)+I_2(\sigma r)}{I_0(\sigma)+I_2(\sigma)} \times (3\sigma^{-\frac{3}{2}}(2\beta_2+5\beta_4)I_1(\sigma) + 2\sigma^{-\frac{1}{2}}\beta_1 I_0(\sigma) + 4\sigma^{\frac{1}{2}}\beta_1 I_1(\sigma) - 4\sigma^{\frac{1}{2}}\beta_3 I_1(\sigma) + 2\beta_1\sigma^{\frac{3}{2}}I_0(\sigma))\right\}\right] + O(\beta\delta^2). \tag{84}$$

Vorticity

The vorticity χ in the boundary layer is given by

$$\left.\begin{aligned}\chi_r &= -\delta\sin\alpha[2f'_{00}+f'_{01}+g'_{01}-\tfrac{1}{2}\zeta g''_{01}+s^2 f'_{02}],\\ \chi_\alpha &= [\beta(2s)^{\frac{1}{2}}]^{-1}[f''_{00}+\delta\cos\alpha(f''_{00}+f''_{01}+s^2 f''_{02})],\\ \chi_s &= -[\delta\sin\alpha/\beta(2s)^{\frac{1}{2}}]\,s g''_{01},\end{aligned}\right\} \tag{85}$$

which decays exponentially away from the wall. Since the boundary layer is thin, the motion in the core will remain irrotational. Figures 4 (*a*) and (*b*) show how the radial and axial vorticities diffuse out in the boundary layer. As the flow develops, the curves become steeper owing to the secondary flow. Both the components are zero in the plane of the bend and their magnitude increases azimuthally, becoming maximum at $\alpha = \frac{1}{2}\pi, \frac{3}{2}\pi$ (upper and lower walls). Figure 4 (*c*) represents the decay of the azimuthal vorticity in the boundary layer. During the initial stages of the motion, the vorticity decays much faster on the inner side of the bend in comparison with the outer side owing to the influence of the external flow on the boundary layer. The graphs are flattened as s increases owing to the decrease in vorticity as in the classical case.

Streamlines in the cross-section

The projection of the streamlines on a cross-section $s = s_0$ of the tube is given by

$$\frac{1}{r}\frac{dr}{d\alpha} = \frac{[u_c+u_b-[\beta/(2s)^{\frac{1}{2}}]\{-\beta_1+\delta\cos\alpha(\beta_3+s^2(2\beta_2+5\beta_4))\}]_{s=s_0}}{[v_c+v_b]_{s=s_0}}, \tag{86}$$

where the suffixes c and b represent the velocity components in the core and the boundary layer respectively. Figures 5 (*a*)–(*d*) show these streamlines for various axial distances as the flow develops further downstream.

The boundary layer of the retarded fluid is growing all round the tube, which results in an accelerated axial motion in the core and (in view of mass conservation) a radial flow converging towards the centre of the cross-section (as in a sink), where the cross-sectional velocity components are zero in the case of a straight

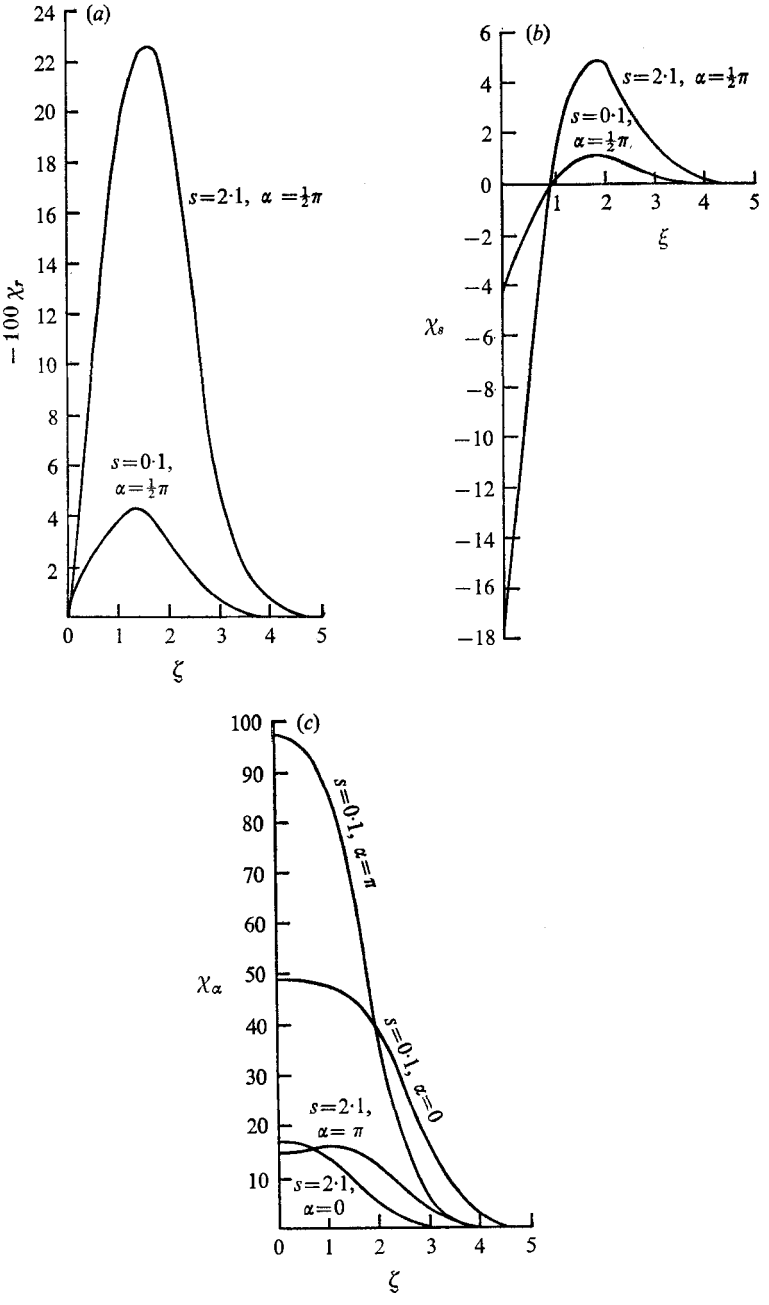

FIGURE 4. (*a*) Radial, (*b*) axial and (*c*) azimuthal vorticity in the boundary layer.

tube. The curvature effect, which is small initially, is that the retarded fluid particles are drawn off azimuthally from the outer side of the bend towards the inner side, which implies that fluid particles are pushed out from the inner side towards the core. Thus the secondary flow enhances the pushing of the fluid particles from the inner part of the bend towards the core. On the other hand,

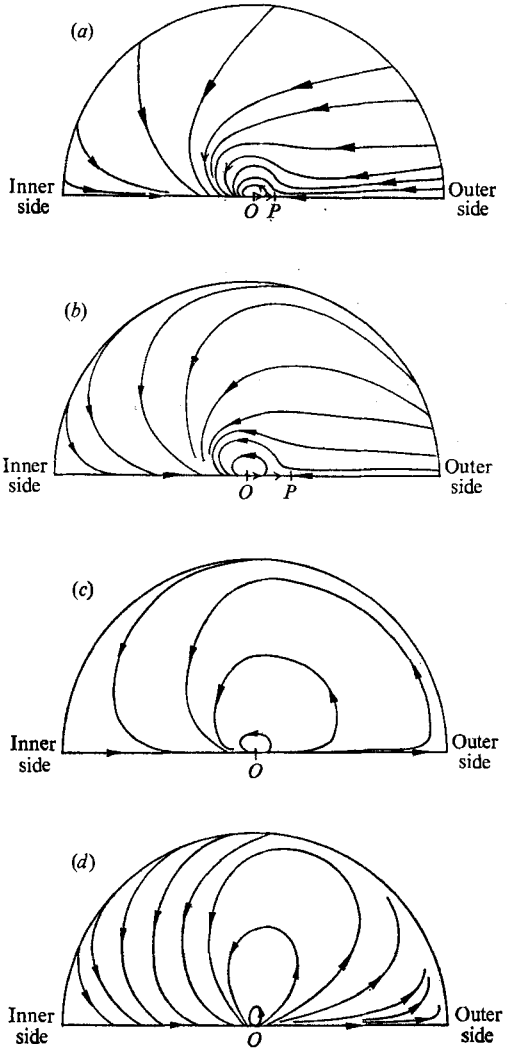

FIGURE 5. Streamlines in cross-sectional planes. (*a*) $s = 0{\cdot}1$, $OP = 0{\cdot}44 \times 10^{-1}$. (*b*) $s = 0{\cdot}6$, $OP = 2{\cdot}27 \times 10^{-1}$. (*c*) $s = 1{\cdot}1$. (*d*) $s = 2{\cdot}1$.

its effect near the outer part will be to diminish continually the pushing of fluid particles until the fluid is entrained by the boundary layer.

This effect is supplemented by a forcing effect occurring within the core as follows. The general acceleration of all the core fluid produces a longitudinal stretching of fluid particles at a greater rate on the inside of the bend (where distances traversed are shorter) than on the outside. This differential stretching sucks fluid from the outside round into the inside, and supplements the boundary-layer displacement effect.

The combination of the two effects induces a movement towards the outside in the plane of symmetry balanced by an opposite movement away from that plane.

The result is that the stagnation point of the cross-sectional flow (which is at $r = 0$ in the case of straight tube) moves along the line of symmetry towards the outer wall as the fluid moves further downstream. At $s = 0{\cdot}1$ (figure 5*a*) this point is at $r = 0{\cdot}044$, and at $s = 0{\cdot}6$ the point shifts to $r = 0{\cdot}227$ (figure 5*b*). This outward shift of the stagnation point continues until the cross-flow from inner to outer wall starts taking place, which occurs when $s \simeq 1$, i.e. equal to the radius of the tube. The azimuthal velocity decreases as the fluid moves further downstream; in the core on the outer side of the bend, it increases away from the line of symmetry with the azimuthal angle, the maximum rate of increase being near the line of symmetry. In the region on the inner side of the bend it decreases as α increases and the rate of decrease is a maximum near the line of symmetry. The radial variation of the azimuthal velocity is negligible. The pattern of the streamlines in the cross-sectional plane is depicted in figures 5(*a*)–(*d*). Mathematically, there are two singularities when s is small: (i) the sink-like origin, which is a node where the streamlines converge (figures 5*a*, *b*), and (ii) the stagnation-type point P, which is a saddle point. The distortion of the streamlines is due to the enhanced/diminished pushing of fluid particles on the inner/outer side of the bend and the azimuthal velocity induced by the curved flow. After the cross-flow has set in, the only singularity will be the nodal point at the origin as shown (figures 5*c*, *d*). The streamlines are stretched as s increases because the azimuthal velocity decreases and radial velocity increases with downstream distance. The slight tilt of the streamlines towards the outer side of the bend is due to the tendency of the fluid particles in the core to move outwards.

Streamwise velocity

Figures 6(*a*) and (*b*) show the accelerating effect of the boundary layer as the flow develops and the gradual outward shift of faster-moving particles which takes place as the streamwise distance increases, which is the effect of the cross-flow in the inviscid core. The behaviour of the contour near $r = 0$ (figure 6*a*) is due to the peculiar behaviour at the origin pointed out earlier.

Figure 7(*a*) shows the linear variation of the streamwise velocity with radial distance. The decrease in velocity from the inner to the outer side of the bend is a maximum in the plane of the bend and gradually becomes smaller until the variation becomes negligible along $\alpha = \frac{1}{2}\pi, \frac{3}{2}\pi$ (the upper and lower walls). This is due to the displacement effect of the boundary layer being influenced by the external flow. The profile at $s = 2{\cdot}0$ indicates a slight increase in the slope, which is the effect of the secondary flow.

Figure 7(*b*) represents the variation of streamwise velocity in the boundary layer. It shows the steeper profile on the inner side of the bend near the entrance region due to the influence of the external flow. The secondary flow steepens the profile on the outer side and flattens it in the inner side, which is reflected in the profiles at $s = 2{\cdot}4$.

Azimuthal velocity

Figure 8(*a*) represents the radial variation of the azimuthal velocity, which is negligible because the flow is irrotational in the core and there is very small

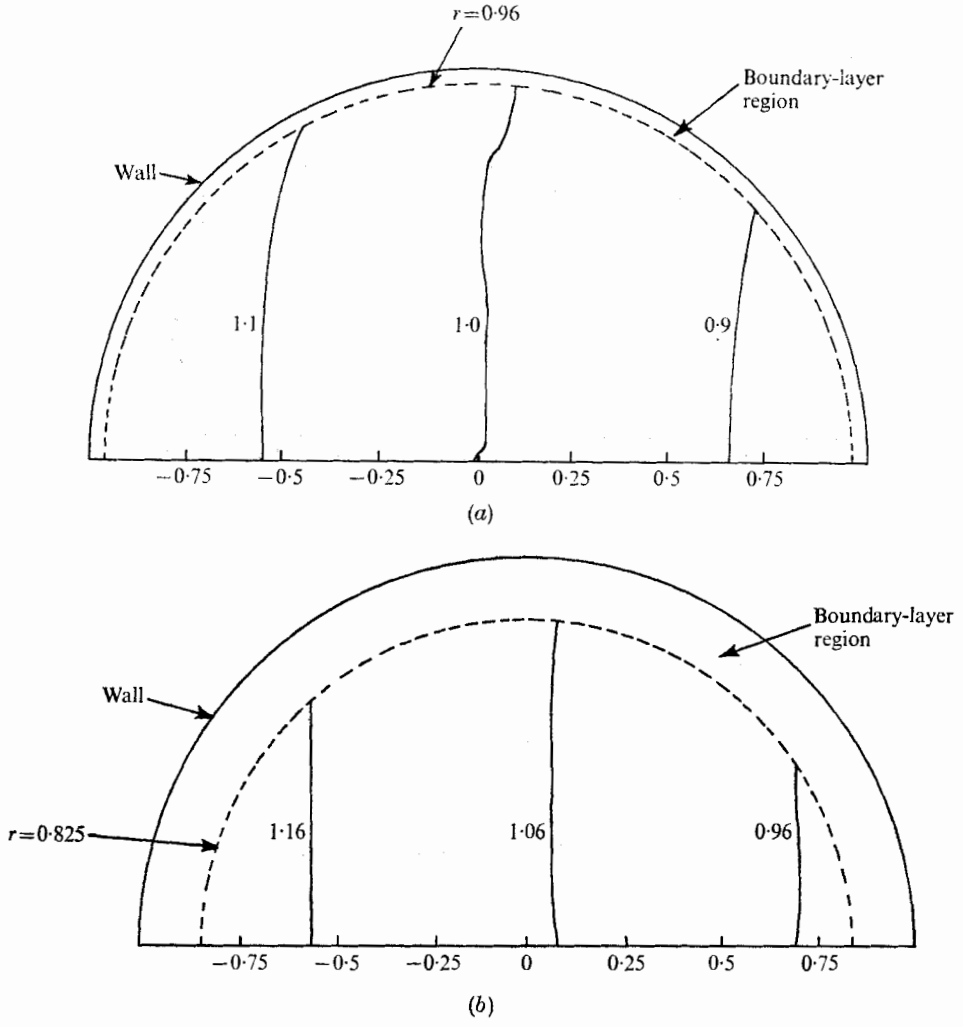

FIGURE 6. Streamwise-velocity contours. (*a*) $s = 0{\cdot}1$. (*b*) $s = 2{\cdot}1$.

azimuthal variation of the radial velocity. The azimuthal velocity is zero in the plane of the bend and increases azimuthally, the maximum velocity being along $\alpha = \frac{1}{2}\pi, \frac{3}{2}\pi$. The velocity decreases continuously as the flow develops.

Figure 8(*b*) shows how the transverse velocity profile in the boundary layer becomes steeper with increasing s.

Pressure drop

Figures 9(*a*) and (*b*) show that, during the initial development of the flow, the pressure distribution is not appreciably influenced by the secondary flow. Figure 9(*a*) shows the linear dependence of the pressure on the radial co-ordinate which occurred at the entry. Figure 9(*b*) represents the pressure drop with the streamwise co-ordinate, which is almost the same as for the entry flow in a straight tube.

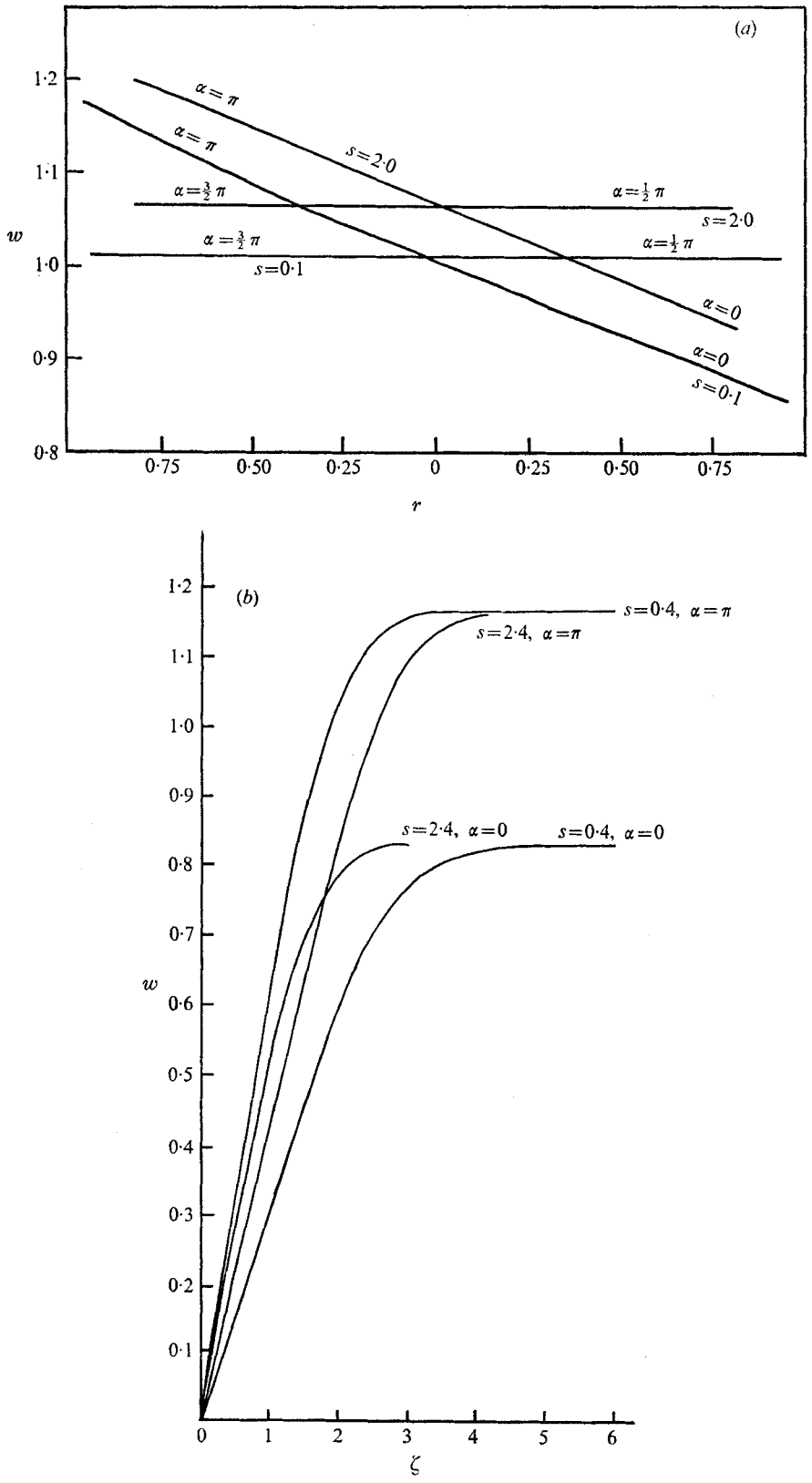

FIGURE 7. Variation of longitudinal velocity (*a*) with radial distance and (*b*) in the boundary layer.

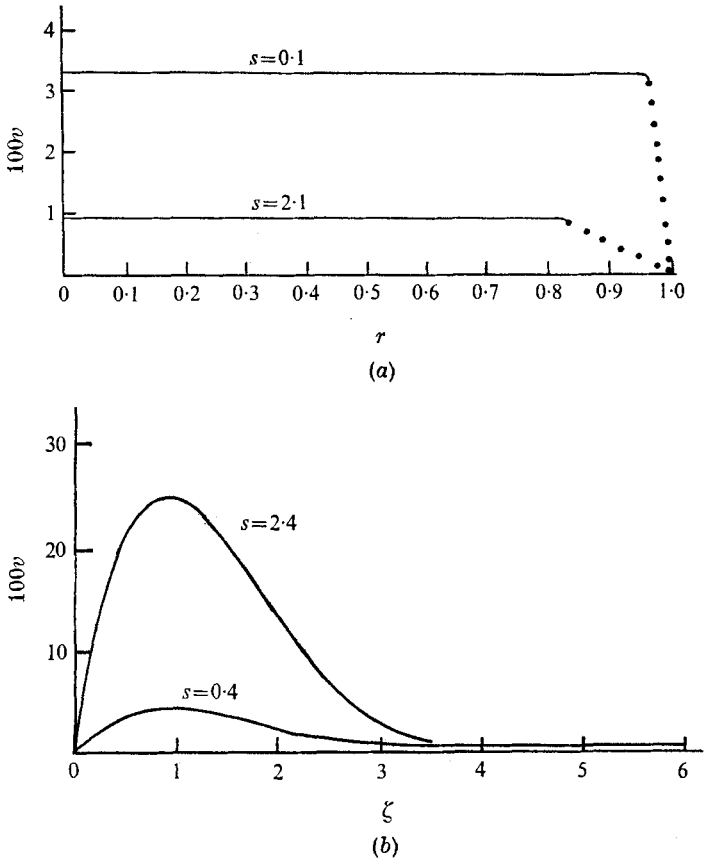

FIGURE 8. (*a*) Radial variation of azimuthal velocity. (*b*) Secondary velocity in the boundary layer $\alpha = \frac{1}{2}\pi$.

Solution for uniform entry

One can check in a straightforward manner that, if the injection velocity is uniform, the results can be obtained from the above analysis by replacing β_3 by $\frac{1}{2}\beta_3$ and f_{01} by $\frac{1}{2}f_{01}$. Besides, the following expansions will hold for p and w in the core:

$$p = \delta r\cos\alpha + O(\delta^2) + \beta[p_{10} + \delta p'_{11}] + O(\beta\delta^2), \tag{87a}$$

where p'_{11} is obtained from (76) by replacing β_3 by $\frac{1}{2}\beta_3$,

$$w = 1 + \beta[w_{10} + \delta w'_{11}] + O(\beta\delta^2), \tag{87b}$$

where w'_{11} is obtained from (77) by replacing β_3 by $\frac{1}{2}\beta_3$. The axial skin friction is given by

$$\begin{aligned}\tau_{ws} &= -(\rho\mu\overline{W}_0^3/2as)^{\frac{1}{2}}[f''_{00}(0) + \delta\cos\alpha\{f''_{00}(0) + \tfrac{1}{2}f''_{01}(0) + s^2 f''_{02}(0)\}]\\ &= -(\rho\mu\overline{W}_0^3/2as)^{\frac{1}{2}}[0{\cdot}4696 + \delta\cos\alpha(0{\cdot}2562s^2 - 0{\cdot}2348)].\end{aligned} \tag{88}$$

The term $0{\cdot}2562s^2$ is solely due to the longer/shorter wall length on the outer/inner side of the bend. In this case, we find that the cross-over occurs at

$$s \simeq 0{\cdot}95, \tag{89}$$

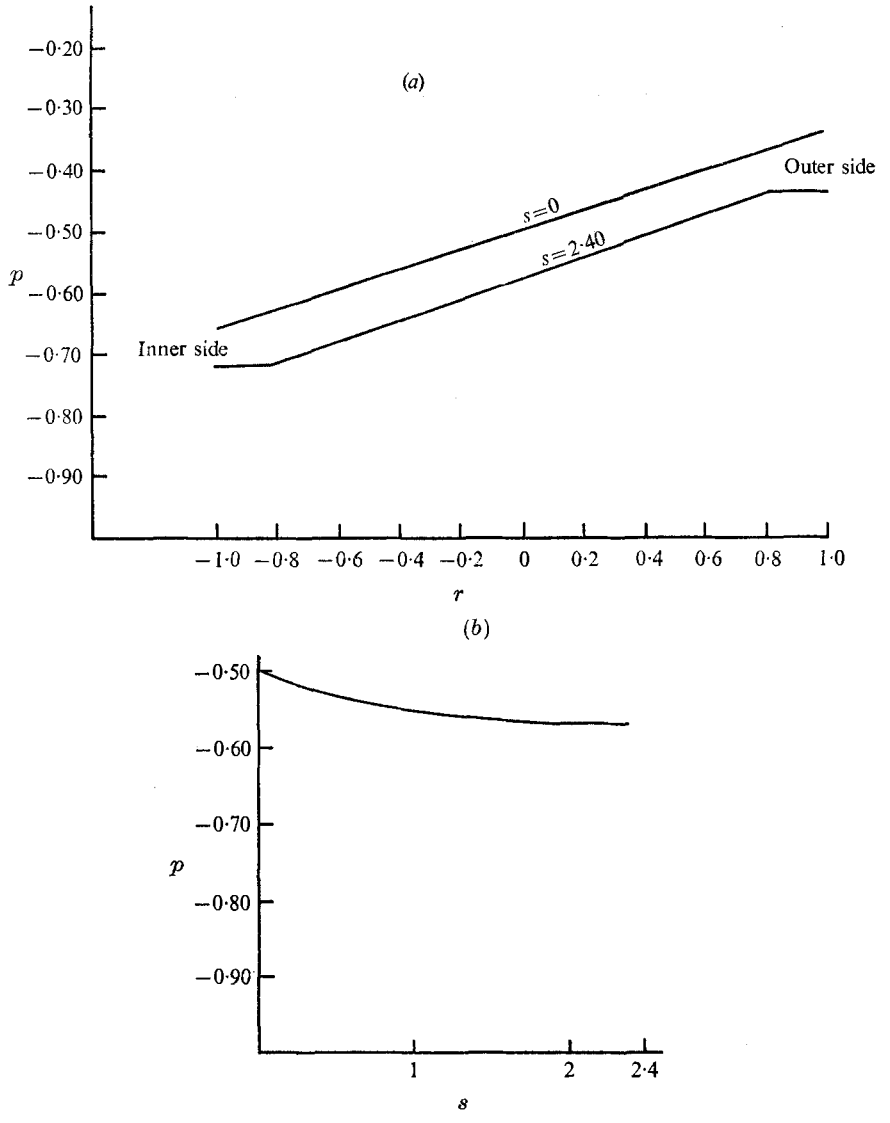

FIGURE 9. (*a*) Pressure *vs.* r in the plane of the bend. (*b*) Pressure *vs.* s along the centre-line.

which is half the distance obtained for the entry condition of constant dynamic pressure. The influence of the entry condition on the initial development of the flow is understandable because comparison of (76) with (88) shows that the frictional resistance on the outer side of the bend is smaller in case (i) (constant dynamic pressure) than in case (ii) (unform entry) because the external velocity $1-\delta r\cos\alpha$ in case (i) is smaller than one, the value in case (ii). Likewise, on the inside of the bend, the external velocity is larger in case (i) and hence the frictional resistance is larger in this case.

Since the new entry condition does not alter the transverse velocity $\tilde{v}_{01}$ in the boundary layer, the azimuthal skin friction will remain the same in the two

cases. However, since the limiting streamlines at the wall depend on the relative order of magnitude of the azimuthal and longitudinal pulling, their positions will not be the same in the two cases. Figure 3 shows that, on the outside of the bend, the streamlines in case (i) are bent more owing to the smaller axial skin friction and on the inside of the bend, streamlines in case (ii) are bent more owing to the smaller axial skin friction in this case. The effect of the curvature ratio shows (figure 3) that the smaller the curvature ratio δ, the smaller is the distortion of the streamlines, which is understandable because the initial flow development in a curved tube is a perturbation of an entry flow in a straight tube. The analysis also shows that the choice of entry condition influences the initial development of the flow but does not significantly affect it further downstream.

The author wishes to express his profound sense of gratitude to Professor Sir James Lighthill F.R.S., Lucasian Professor, who suggested the problem, for the privilege of having several inspiring discussions with him and his continued interest throughout the preparation of this work. Thanks are also due to Dr T. J. Pedley for useful discussions. This work was carried out while the author was on leave from IIT, Delhi under the exchange programme between IIT, Delhi and the British Universities, under the auspices of the Imperial College Delhi Committee, London.

REFERENCES

ADLER, M. 1934 *Z. angew. Math. Mech.* **14**, 257.

BARUA, S. N. 1963 *Quart. J. Mech. Appl. Math.* **16**, 61.

CARO, C. G., FITZ-GERALD, J. M. & SCHROTER, R. C. 1969 *Nature*, **223**, 1159.

DEAN, W. R. 1927 *Phil. Mag.* **4**, 208.

DEAN, W. R. 1928 *Phil. Mag.* **5**, 673.

GOLDSTEIN, S. 1965 Unpublished work described in *Modern Developments in Fluid Dynamics*, vol. 1. Dover.

GREENSPAN, D. 1973 *J. Fluid Mech.* **57**, 167.

HAWTHORNE, W. R. 1951 *Proc. Roy. Soc.* A **206**, 374.

KUCHAR, N. R. & OSTRACH, S. 1967 Unsteady laminar flows in elastic tubes with applications to the vascular system. *Case Western Reserve University (Cleveland, Ohio) Rep.* FTAS/TR-67-25.

MCCONALOGUE, D. J. & SRIVASTAVA, R. S. 1968 *Proc. Roy. Soc.* A **307**, 37.

MCDONALD, D. A. 1960 *Blood Flow in Arteries.* London: Arnold.

NEREM, R. M. & SEED, W. A. 1972 *Cardiovascular Res.* **6**, 1.

OLSON, D. E. 1971 Fluid mechanics relevant to respiratory flow within curved or elliptic tubes and bifurcating system. Ph.D. thesis, Imperial College, London.

PICKETT, G. F. 1968 Incompressible viscous flow in a curved pipe. Ph.D. thesis, Imperial College, London.

SEED, W. A. & WOOD, N. B. 1971 *Cardiovascular Res.* **5**, 319.

THOMPSON, J. 1876 *Proc. Roy. Soc.* **28**, 5.

VAN DYKE, M. 1970 *J Fluid Mech* **44**, 813.

WHITE, C. M. 1929 *Proc. Roy. Soc.* A **123**, 645.

WILSON, S. D. R. 1971 *J. Fluid Mech.* **46**, 787.

YAO, L. 1973 Entry flow in a curved pipe. Ph.D. thesis, University of California, Berkeley.